ChemistrySelect

Research Article
doi.org/10.1002/slct.202502039

Chemistry Europe
European Chemical Societies Publishing

www.chemistryselect.org

The Halogen Effect in [Cu(NHC)X] Compounds: A Case Study on the Anti-*Leishmania* and Antiviral Activity of [Cu(IPr)X]

J. V. Fontes[†],[a] M. E. F. Agnoli[†],[a] G. Clauss,[a] M. S. A. Garcia,[b] A. V. P. Ferreira,[b] G. A. Antoniucci,[c] A. L. Costa-Oliveira,[c] A.C.G. Jardim,[c, d] D. C. Miguel,[b] and C. Abbehausen*[a]

In this study, we investigated the activity and properties of three neutral Cu(I) *N*-heterocyclic carbene (NHC) complexes—[1,3-bis(2,6-diisopropylphenyl) imidazol-2-ylidene]copper(I) with Cl, Br, and I, specifically **[Cu(IPr)Cl]**, **[Cu(IPr)Br]**, and **[Cu(IPr)I]**—to evaluate the impact of halogen substitution on anti-*Leishmania* and antiviral activity. The compounds were synthesized using reported methods. ^{13}C NMR spectroscopy provided insights into the electronic nature of the Cu—X bond by analyzing the NHC C^2 chemical shift. Notably, the iodine derivative exhibited distinct chemical properties compared to its counterparts, displaying a more covalent Cu—I bond. As a result, **[Cu(IPr)I]** was more susceptible to nucleophilic attack, as confirmed by HOMO–LUMO gap calculations using DFT. Furthermore, this derivative demonstrated the highest lipophilicity and the strongest antioxidant activity in the series, as evidenced by the DPPH assay, surpassing butylated hydroxytoluene (BHT) used as a positive control. Bovine serum albumin (BSA) binding assays indicated weak interaction (10^3 M^{-1}) across all compounds, with no significant differences observed. In anti-*Leishmania* assays, **[Cu(IPr)I]** exhibited the best selectivity index (SI = 4.0), showing greater toxicity to the parasite (EC_{50} = 1.5 μM) while being less toxic to the host cell (CC_{50} = 6.0 μM). However, this trend did not extend to antiviral studies against the chikungunya virus, where **[Cu(IPr)Br]** displayed the highest replication inhibition (EC_{50} = 0.807 μM) and the best selectivity index (SI = 4.8). Our findings highlight that halogen substitution plays a crucial role in modulating the biological activity of neutral linear metal-NHC complexes.

1. Introduction

According to the World Health Organization (WHO), neglected tropical diseases (NTDs) are caused by parasites, bacteria, fungi, viruses, or non-communicable origin, predominantly affecting populations in tropical and subtropical regions. These diseases are often endemic or epidemic, remain difficult to control, lack effective vaccines or other preventative measures, and pose significant health and economic burdens.[1]

Among more than 20 recognized NTDs, leishmaniasis still poses a great challenge in 88 countries. Caused by over 20 protozoa species that belong to the genus *Leishmania*, their flagellated forms (promastigotes) are transmitted through the bite of infected sand flies to several mammalian hosts, including humans, wherein they transform into proliferative amastigotes in mononuclear phagocytic cells, leading to distinct clinical manifestations.[1,2]

Two classic forms of leishmaniasis are recognized: cutaneous (CL) and visceral leishmaniasis (VL). Current treatments are based on intravenous administration of pentavalent antimonials (sodium stibogluconate and meglumine antimoniate), liposomal amphotericin B, miltefosine, and paromomycin. Despite their effectiveness, these painful treatments are associated with severe side effects, require hospitalization, and can be financially prohibitive, as seen for liposomal amphotericin B, which despite being effective, is limited for large-scale public health use due to its high cost.[3]

Another significant group of NTDs includes arboviral infections, such as dengue, chikungunya, Mayaro, and Zika fevers. Among them, this work focuses on chikungunya virus (CHIKV), the causative agent of chikungunya fever, an arthropod-borne viral disease primarily transmitted by *Aedes aegypti* in urban areas and *Aedes albopictus* in rural or wild environments.[4–6] CHIKV infection is characterized by high fever, rash, and severe arthralgia, which, in many cases, progresses into a

[a] *J. V. Fontes[†], M. E. F. Agnoli[†], G. Clauss, C. Abbehausen*
Institute of Chemistry, University of Campinas–UNICAMP, PO Box 6154, Campinas, SP 13083-970, Brazil
E-mail: camilla@unicamp.br

[b] *M. S. A. Garcia, A. V. P. Ferreira, D. C. Miguel*
Institute of Biology, University of Campinas–UNICAMP, Campinas, SP 13083-862, Brazil

[c] *G. A. Antoniucci, A. L. Costa-Oliveira, A. Jardim*
Institute of Biomedical Sciences, Federal University of Uberlândia, Uberlandia, MG, Brazil

[d] *A. Jardim*
Institute of Biosciences, Humanities and Exact Sciences (Ibilce), São Paulo State University (Unesp), Campus São José do Rio Preto, São José do Rio Preto, SP, Brazil

[†] *Both authors contributed equally to this work.*

Supporting information for this article is available on the WWW under https://doi.org/10.1002/slct.202502039

chronic debilitating condition that persists for months or even years. Despite the significant public health burden, no antiviral drugs or vaccines are currently approved for CHIKV prevention or treatment. The standard clinical approach remains symptomatic management, underscoring the urgent need for effective antiviral therapies to reduce disease severity and long-term complications.[7]

Our research group has been exploring metal-based compounds as potential therapeutics for NTDs, including leishmaniasis, Chagas disease, and arboviral infections.[1,8–12] We focus on rational ligand design to establish structure-activity relationships in our search for improved metal-based drug candidates. In particular, we have been investigating gold(I) complexes with *N*-heterocyclic carbenes (NHCs),[10,12] and by analogy, copper(I)-NHC complexes.

Copper is an essential trace element in humans, and its intrinsic toxicity can be mitigated by the body's natural mechanisms for copper transport and storage.[13] In biological systems, copper exists predominantly in the Cu(I) and Cu(II) oxidation states and plays critical roles in ATP synthesis, redox reactions, neurological function, heme biosynthesis, and iron metabolism.[14] Cu(I) is considered a soft acid according to Pearson's classification and preferentially coordinates to soft bases, forming linear, trigonal planar, or tetrahedral complexes—features that make Cu(I) complexes attractive for medicinal applications targeting thiol- and selenol-containing biomolecules.[15]

N-Heterocyclic carbenes are excellent ligands for stabilizing Cu(I), forming robust, linear complexes. Their strong σ-donor and significant π-acceptor properties allow for fine-tuning of complex characteristics, including lipophilicity, ligand exchange kinetics, and redox stability.[16] Despite these favorable properties, the medicinal potential of Cu(I)-NHC complexes remains less explored compared to their Ag(I)- and Au(I)-NHC counterparts. Literature reports indicate that Cu(I)-NHC complexes exhibit promising biological activity, with low inhibitory concentrations against tumor cells, *Leishmania major*, *Candida albicans*, methicillin-resistant *Staphylococcus aureus* (MRSA), and other bacteria.[17–20]

Our group has also been investigating both Cu(II)[21] and Cu(I)-NHC[20] complexes as potential leishmanicidal and antiviral agents. In our initial studies, we demonstrated that [1,3-bis(2,4,6-trimethylphenyl)imidazol-2-ylidene]copper(I) with chloride [Cu(IMes)Cl], undergoes speciation in solution, affecting biological outcomes, while [Cu(IPr)Cl] remains stable and exhibits superior biological activity, with a favorable selectivity index against *Leishmania amazonensis* and up to 91% inhibition of chikungunya virus (CHIKV) replication. Despite these promising results, cytotoxicity toward host cells limits testing to concentrations below 3 μM.[21]

Numerous studies have demonstrated that the substitution of chloride with iodide in metal complexes can significantly enhance both biological activity and selectivity.[22–25] In our investigations, we have observed a marked improvement in antitumor activity in Pd(II) complexes upon coordination with iodide.[24] Despite these findings, the majority of halide NHC-metal(I) complexes predominantly feature chloride or bromide as the leaving group, with only a limited number of studies exploring the biological activities of Cl, Br, and I.[18,19,26] Furthermore, only two studies specifically address the correlation between the reactivity of different halogens and their biological effects.[27,28]

In this study, we investigate the leishmanicidal and antiviral properties of a series of **[Cu(I)(IPr)X]** complexes (X = Cl, Br, I). Remarkably, iodine substitution significantly enhanced the selectivity index against *L. amazonensis*, indicating improved antiparasitic potential. In contrast, antiviral (CHIKV) assays revealed **[Cu(IPr)Br]** as the most selective compound, highlighting distinct structure–activity trends. To better understand these differences, we examined the lipophilicity and electronic features of the Cu—X bonds, along with total antioxidant capacity and interactions with bovine serum albumin (BSA). These findings provide valuable insights for the rational design of multifunctional copper-based therapeutics.

2. Experimental Section

2.1. Materials and Equipment

All syntheses were carried out under air without any precautions to avoid oxygen and humidity. The solvents were acquired and used as received without further purification (Aldrich, Synth, or LS Chemicals). The ligand IPr.HCl was synthesized using a method previously described.[29] Elemental analysis (CHNS) was acquired using a Perkin–Elmer 2400 CHNS/O elemental analyzer. Nuclear magnetic resonance (NMR) ^{1}H and ^{13}C spectra were obtained from Bruker equipment, Avance DPX 250 MHz, or Avance III 500 MHz models. Absorption spectra in the UV–vis region were obtained in the HP 8453 UV–vis Agilent spectrophotometer in a 10 mm optical path 3 mL cuvette. Fluorescence spectra were performed using an Agilent Cary Eclipse fluorescent spectrophotometer with a 3 mL and 10 mm optical path cuvette.

2.2. Synthesis

2.2.1. Synthesis of Ligand 1,3-Bis(2,6 diisopropylphenyl)imidazolium Chloride (IPr.HCl) (1)

Synthesis was carried out according to the methodology of Hans et al.[29] The compound was obtained in two steps. The first step was the synthesis of *N*,*N*″-bis(2,6-diisopropylphenyl)ethylenediimine. A solution of glyoxal (70% v/v aqueous, 1.6 mL, 68.41 mmol) in isopropanol was mixed with a solution of 2,6-diisopropylaniline (68.41 mmol, in isopropanol). The resulting solution was stirred for 24 h at room temperature. After the filtration, the yellow solid was dried in an IR lamp. In the next step, paraformaldehyde was added to a solution of *N*,*N*″-bis(2,6-diisopropylphenyl)ethylenediimine in ethyl acetate at 70 °C and vigorously stirred for 45 min. Afterward, a solution of chlorotrimethylsilane in ethyl acetate was added, and the resulting solution was stirred for 2 h and stored at 6 °C overnight. The white solid was filtered and washed with ethyl acetate and ethyl ether and dried under an IR lamp to afford pure 1,3-bis(2,6-diisopropylphenyl)imidazolium chloride as a white microcrystalline powder. (Yield: 70%, 1.95 g, 4.57 mmol).

^{1}H NMR (250 MHz, $CDCl_3$): δ 1.15–1.27(d, $^{3}J_{H\text{-}H}$ = 6.8 Hz, 24H, $CH(CH_3)_2$), 2.30–2.40 (sept, $^{3}J_{H\text{-}H}$ = 6.8 Hz, 4 H, $CH(CH_3)_2$), 7.51–7.54 (d, $^{3}J_{H\text{-}H}$ = 7.8 Hz, 4H, m-CH Dip),7.66–7.72 (t, $^{3}J_{H\text{-}H}$ = 7.7 Hz, 2 H, p-CH Dip), 8.58 (s, 2 H, $CH^{4,5}$ Im), 10.30 (s, 1 H, CHIm).

2.2.2. Synthesis of Complex [Cu(IPr)X] Where X = Cl, Br, and I

The general procedure was carried out following the methodology described by Santoro et al.[30] The ligand IPr.HCl(1) (1.0 equiv), CuX (1.0 equiv), and K_2CO_3 (2.0 equiv) were stirred in acetone (4.0 mL) at 60 °C for 24 h. The reaction mixture was subsequently filtered through silica and washed with dichloromethane, and the filtrate was concentrated under reduced pressure. The addition of pentane (3.0 mL) induced the precipitation of the target compound, which was isolated by filtration, washed with additional portions of pentane, and dried under vacuum. The resulting solid was recrystallized using an acetone/diethyl ether solvent system, affording the final product.

2.2.3. [1,3-Bis(2,6-diisopropylphenyl)imidazol-2-ylidene]copper(I) Chloride [Cu(IPr)Cl] (2)

White solid (Yield: 63%, 71.8 mg, 0.15 mmol). MW: 487.595 g/mol CHN Calc $C_{27}H_{36}N_2ClCu$. %: C 66.56; H 7.45; N 5.75. Found % C 66.51; H 7.44; N 5.75. ^{1}H NMR (600 MHz, DMSO-d_6): δ 1.20–1.22 (d, $^3J_{H-H}$ = 6.8 Hz, 24H), 7.39–7.43 (d, $^3J_{H-H}$ = 7.4 Hz, 4H), 7.53–7.59 (t, $^3J_{H-H}$ = 8.3 Hz, 2H), 7.89 (s, 2H). ^{13}C NMR (150.9 MHz, DMSO-d_6): 23.83 (CH_3), 24.86 (CH_3), 28.72 (CH_3), 124.45 (C^4 and C^5 Im), 124.91 (CH Ar), 130.74 (s, C Ar), 134.92 (C Ar), 145.76 (CH Ar), 178.74 (C^2 Im). HRMS (acetonitrile) = *m/z*: 492.2442.

2.2.4. [1,3-Bis(2,6-diisopropylphenyl)imidazol-2-ylidene]copper(I) Bromine [Cu(IPr)Br] (3)

White solid (yield: 68%, 84.9 mg, 0.16 mmol) MW: 532.049 g/mol CHN Calc. $C_{27}H_{36}N_2BrCu$ %: C 60.95; H 6.82; N 5.27. Found % C 62.06; H 6.70; N 5.34. ^{1}H NMR (600 MHz, DMSO-d_6): δ 1.20–1.21 (d, $^3J_{H-H}$ = 6.8 Hz, 24H), 7.40–7.42 (d, $^3J_{H-H}$ = 7.8 Hz, 4H), 7.54–7.65 (t,$^3J_{H-H}$ = 7.8 Hz, 2H), 7.90 (s, 2H). ^{13}C NMR (150.9 MHz, DMSO-d_6): 23.34 (CH_3), 24.37 (CH_3), 28.21 (CH_3), 123.93 (C^4 and C^5 Im), 124.38 (CH Ar), 130.23(s, C Ar), 134.37 (C Ar), 145.25 (CH Ar), 179.00 (C^2 Im). HRMS (acetonitrile) = *m/z*: 492.2442.

2.2.5. [1,3-Bis(2,6-diisopropylphenyl)imidazol-2-ylidene]copper(I) Iodide [Cu(IPr)I] (4)

Pale yellow solid (yield: 78%, 105.7 mg, 0.18 mmol). MW: 579.049 g/mol CHN Calc. $C_{27}H_{36}N_2CuI$ %: C 56.01; H 6.27; N 4.84. Found % C 55.86; H 6.01; N 4.81. ^{1}H NMR (600 MHz, DMSO-d_6): δ 1.20–1.22 (t, $^3J_{H-H}$ = 6.6 Hz, 24H), 7.40–7.41 (d, $^3J_{H-H}$ = 7.8 Hz, 4H), 7.53–7.60 (t, $^3J_{H-H}$ = 7.8 Hz, 2H), 7.90 (s, 2H). ^{13}C NMR (150.9 MHz, DMSO-d_6): 23.42 (CH_3), 24.37 (CH_3), 28.22 (CH_3), 123.90 (C^4 and C^5 Im), 124.30 (CH Ar), 130.22(s, C Ar), 134.33 (C Ar), 145.27 (CH Ar), 180.91 (C^2 Im). HRMS (acetonitrile) = *m/z*: 492.2442, 939.3990.

2.3. Ligand Exchange Kinetics Followed by ^{1}H NMR

The experiment was conducted applying the same conditions as reported by Fontes et al.,[20] which studied the stability of the complex **[Cu(IPr)Cl]**.

In 750 µL of DMSO-d_6 or DMSO-d_6/D_2O (13:1), 4 mg of the compounds **[Cu(IPr)Br]** and **[Cu(IPr)I]** were added, which were transferred to NMR tubes. The ^{1}H NMR (500 MHz) spectrum was obtained at the time the solutions were prepared (time 0 h). The NMR tubes were kept at a constant temperature of 25 °C for the subsequent measurements of 3, 6, 8, 24, and 48 h in DMSO-d_6 and DMSO-d_6/D_2O (13:1).

2.4. High-Resolution Mass Spectrometry

High-resolution mass spectra (HRMS) were recorded on an Orbitrap Thermo QExactive mass spectrometer equipped with an electrospray ionization (ESI) source operating in positive ion mode. The samples were dissolved in acetonitrile at a concentration of 1 mg/mL and introduced via direct infusion at a flow rate of 200 µL/min ACN:H_2O 1:1 v/v.

2.5. Antioxidant Activity: DPPH Radical

Stock solutions of the complexes and BHT (1×10^{-4} M) were prepared in ethanol with 10% DMSO (V/V) and protected from light. A fresh DPPH (1×10^{-4} M) solution in ethanol was also shielded from light. In a 10 mm quartz cuvette, 1.0 mL of DPPH solution was mixed with 1.0 mL of the sample or DMSO (control). The absorbance was measured by spectroscopy in the ultraviolet/visible region (UV–vis), at the wavelength 517 nm, after 60 min of reaction of the samples (A_{sample}) and control (A_{DPPH}). All analyses were done in triplicate. The antioxidant capacities were expressed as a percentage reduction of DPPH$^{\cdot}$ (Equation 1).

$$\%\text{Reduction} = \frac{\left(A_{\text{DPPH}\cdot} - A_{\text{sample}}\right) \times 100}{A_{\text{DPPH}\cdot}} \quad (1)$$

2.6. Bovine Serum Albumin Interaction with Complexes: Fluorescence Quenching

Solutions of the complexes (1.5 mM) were prepared in DMSO, while BSA (20 µM) was prepared in phosphate buffer (10 mM, pH 7.4). The albumin solution was titrated with 8 µL increments of copper complexes, and fluorescence spectra (excitation: 280 nm, emission: 300–400 nm) were recorded after 1 min. Measurements were performed at 25 °C.

The emission intensity at 350 nm was evaluated by the Stern–Volmer equations. The Stern–Volmer constant (K_{SV}) was obtained by Equation (2), where I_0 and I are the relative fluorescence intensities of BSA in the absence and presence of the quencher, respectively, and [Q] is the quencher concentration.

$$I_0/I = 1 + K_{SV}[Q] \quad (2)$$

Scatchard Equation (3) was used to evaluate the number of sites (n) and the equilibrium constant between free and bound molecules (K_b) of complexes **[Cu(IPr)Cl]**, **[Cu(IPr)Br]**, and **[Cu(IPr)I]**.

$$\log\left(I_0 - I\right)/I = \log K_b + n\log[Q] \quad (3)$$

2.7. Lipophilicity

The logarithmic partition coefficient (log P) of the copper complexes was determined using the shake flask method, following OECD guidelines with modifications.[31,32] Complexes were dissolved in Milli-Q water (pre-saturated with 1-octanol) to prepare 0.1 mM stock solutions, then mixed with an equal volume of *n*-octanol (pre-saturated with water) and shaken for 2 h at room temperature. After phase separation by centrifugation, experiments were conducted in duplicate. The initial and final aqueous phases were acid-digested (50% HNO_3), calcinated (500 °C, 20 min), and dissolved in 1% HNO_3 (Merck, ICP grade) for ICP-OES analysis. The partition coefficient was obtained considering $[Cu]_{octanol} = [Cu]_{total} - [Cu]_{water}$ and

calculated according to Equation (4).

$$\log P = \frac{[Cu]_{octanol}}{[Cu]_{water}} \quad (4)$$

2.8. Computational details

The copper complex structures were optimized using density functional theory (DFT) calculations with the ORCA v. 6.0 package.[36] Geometry optimizations were performed with the ωB97X-D3BJ functional,[37] employing the SARC-ZORA-TZVP basis set for iodine, ZORA-def2-TZVP for all other atoms, and SARC/J auxiliary basis functions,[38] along with the RIJCOSX approximation.[39] Implicit solvation in DMSO was considered using the CPCM model.[40,41]

A convergence criterion of 1.0×10^{-8} a.u. was applied. Frequency calculations, performed at the same theoretical level, confirmed the optimized structures as true minima (absence of imaginary frequencies) and provided thermodynamic data at 298.15 K. Bader atomic charges were calculated using the Multiwfn program,[42] based on the electronic densities obtained from the optimized structures. The frontier orbital energies of the complexes were also analyzed.

2.9. Anti-*Leishmania* Evaluation

2.9.1. Parasite Culture

The promastigote forms of *L. amazonensis* (IFLA/BR/67/PH8) was kindly donated by Dr Norma Andrews (UMD, USA) and cultured at 25 °C in 25 cm^2 culture bottles containing promastigote growth medium: M199 (Gibco BRL) pH 7.4 supplemented with 10% heat-inactivated fetal bovine serum–FBS (Invitrogen), 5% penicillin/streptomycin, 0.1% hemin (25 mg/mL in 50% triethanolamine), 10 mM adenine (pH 7.5), and 5 mM L-glutamine, as previously described.[33] Cultures were split every 5 days, after promastigotes reached late logarithmic growth phase.

2.9.2. Extraction of Primary Host Cell

Bone marrow-derived macrophages (BMDM) were obtained after differentiation of precursor cells extracted from femurs and tibias of female Balb/C mice. The medullary cavities of the bones were washed with a 5 mL syringe and a 21G needle with Roswell Park Memorial Institute (RPMI 1640) medium (Gibco-Invitrogen) supplemented with 20% FBS and 30% L929 fibroblast culture supernatant in 75 mm Petri dishes. Recovered cells were kept at 37 °C with 5% CO_2 atmosphere. After 7 days, differentiated BMDM were collected with fresh RPMI medium after scraping the plate with a sterile cell scraper (Biofil). The Ethics Committee on Animal Use of the University of Campinas (CEUA/UNICAMP, protocol #6022–1/2022) approved all procedures using mice.

2.9.3. Cell Viability Assays

Cell viability was evaluated by the MTT ((3-(4,5-dimethylthiazol-2-yl)-2,5-diphenyltetrazolium bromide) assay[34] using log phase *Leishmania* promastigote cultures (5×10^6 cells/well) or BMDM (5×10^4 cells/well) in 96-well culture plates incubated with decreasing concentrations of the Cu complexes (25; 12.5; 6.25; 3.13; 1.56; 0.78; 0.4 e 0 µM) for 24 h. All complexes were freshly solubilized in pure sterile DMSO (Sigma–Aldrich) at 10 mM stocks for each experiment. Briefly, 30 µL of MTT (5 mg·mL^{-1}) was added to each well, and the plates were incubated for 3 h at 25 °C (for promastigotes) and 37 °C (for macrophages). Next, the reaction was stopped by the addition of 30 µL of SDS 20%. Absorbance reading was performed using a plate spectrophotometer (reference and test wavelengths of 600 and 650 nm, respectively). Optical density values were converted to percentages compared to untreated control groups incubated with medium only (100% viability) to determine the 50% effective concentrations (EC_{50} for parasites and CC_{50} for macrophages) from sigmoidal regression of dose-response curves (GraphPad Prism8 software, USA). The results obtained were compared in terms of the selectivity index (SI) calculated for each compound ($SI = CC_{50}/EC_{50}$).

2.10. Antiviral Studies

2.10.1. Cell culture

The Vero-E6 cell were maintained in Dulbecco's modified Eagle's medium (DMEM, Sigma–Aldrich) supplemented with 100 U/mL of penicillin (Sigma–Aldrich), 100 mg/mL of streptomycin (Sigma–Aldrich), 1% dilution of stock of non-essential amino acids (Sigma–Aldrich), 5% of fetal bovine serum (FBS, Cultilab), incubated at 37 °C and 5% CO_2.

2.10.2. Cell viability assay

Cell viability was measured by MTT [3-(4,5-dimethylthiazol-2-yl)-2,5-diphenyl tetrazolium bromide] (Sigma–Aldrich) assay. Vero-E6 cells were cultured in a 48-well plate at 5×10^4 cells/well and treated with six different concentrations of compounds, ranging from 0.016 µM to 50 µM, for 24 h at 37 °C with 5% of CO_2. After 24 h post-treatment, media containing compound was removed, and MTT at 1 mg/mL solution was added to each well, incubated for 30 min, and replaced with 300 µL of DMSO to solubilize the formazan crystals. The absorbance was measured at 560 nm on Glomax microplate reader (Promega). Cell viability was calculated according to the equation $(T/C) \times 100\%$, where *T* and *C* represented the optical density of the treated well and control groups, respectively. The cytotoxic concentration of 50% inhibition (CC_{50}) was calculated using GraphPad Prism 8.0.

2.10.3. Antiviral assays

To assess the antiviral activity of compounds, Vero-E6 cells were seeded at a density of 5×10^4 cells per well into 48-well plates. After 24 h, cells were infected with CHIKV-*nanoluc*[35] and treated with different concentrations, ranging from 0.016 µM to 50 µM, at 37 °C with 5% of CO_2. 24 h post-treatment, samples were harvested using *Renilla*-luciferase lysis buffer (Promega), and virus replication levels were quantified by measuring *Renilla*-luciferase activity using the *Renilla* Luciferase Assay System (Promega). The antiviral activity was calculated according to the equation $(T/C) \times 100\%$, where T and C represent the mean of the treated group and mean of the last concentration, respectively. The effective concentration of 50% inhibition (EC_{50}) was calculated using GraphPad Prism 8.0. The values of CC_{50} and EC_{50} were used to calculate the selectivity index ($SI = CC_{50}/EC_{50}$).

2.10.4. Statistical analysis

Individual experiments were performed in triplicate, and all assays were carried out a minimum of three times to confirm reproducibility. GraphPad Prism 8.0 software was used to assess statistical

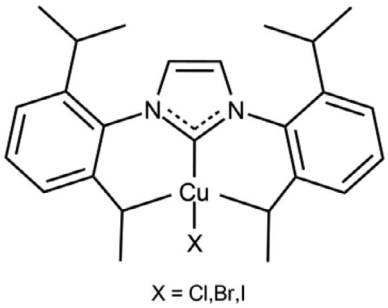

Figure 1. Structural formula discussed in this work [Cu(IPr)X] (X = Cl, Br, and I).

differences of means of readings. The EC_{50} and CC_{50} were calculated using a non-linear regression considering log(inhibitor) versus response, with variable slope (four parameters–$p < 0.05$).

3. Results and Discussion

3.1. Synthesis and Spectroscopic Characterization

Ligand IPr.HCl and complexes **[Cu(IPr)Cl]**, **[Cu(IPr)Br]**, and **[Cu(IPr)I]** were successfully synthesized (Figure 1). Among all the diverse methodologies of symmetric imidazol-2-ylidene, in this work, we followed one of the most atom-economical and straightforward paths.[30,43] The complexes were prepared following the "weak base" method by Santoro and coworkers[30] involving the reaction of IPr·HCl with the respective CuX salt in acetone and two equivalents of K_2CO_3. Their group demonstrated that this reaction pathway is highly effective, as only two halide species were observed when the reaction was conducted in the absence of a base. Upon addition of that, the reaction profile changed immediately, highlighting the significant influence of basic conditions on the reaction outcome. Under these conditions, only the halide corresponding to the CuX salt was detected, suggesting that the base plays a key role in determining halide species in the complex. Elemental analysis confirms the composition, and the structure was analyzed by ^{1}H and ^{13}C NMR, HR ESI-MS.

The spectra of ^{1}H NMR of compounds IPr.HCl, **[Cu(IPr)Cl]**, **[Cu(IPr)Br]**, and **[Cu(IPr)I]** are shown in Figures S1–S4 (Supporting Information). All of them agree with the reports in the literature.[29,30] The complexe's elemental analysis, ^{13}C NMR spectra (Figures S4–S8) show the compounds were pure. Stability tests were performed by 1H NMR spectra in DMSO-d_6 and DMSO-d_6:D_2O 13:1 (v/v) and showed no change over time up to 48 h (Figures S9–S12). The formation of [Cu(IPr)X] was also confirmed by HR ESI-MS (Figure S13–S15).

The ^{1}H NMR spectrum of the ligand IPr•HCl displays two doublets between 1.24 and 1.73 ppm, attributed to the methyl protons, and a multiplet at 2.35 ppm corresponding to the CH protons. Aromatic protons appear in the region of 7.5–7.7 ppm. The imidazole ring protons at positions 4 and 5 appear as a singlet at 8.58 ppm, while the proton at position 2 (C^2—H) is observed as a singlet at 10.23 ppm. The primary evidence for complex formation is the disappearance of the C^2—H signal at 10.23 ppm in the ^{1}H NMR spectra of the complexes, confirming carbene coordination to the copper center. Additional spectral changes support this transformation: the methyl protons appear as a single doublet at 1.2 ppm, the CH protons shift to 2.5 ppm (overlapping with the DMSO solvent signal), and the imidazole 4 and 5 protons shift to 7.9 ppm. These shifts are consistent across all complexes, indicating similar coordination environments.

The ^{13}C NMR spectra of the complexes exhibit chemical shifts that are similar to those of the free ligand, except the imidazole C^2 signal. In the free ligand, this carbon is readily detected at 144.8 ppm. In the metal complexes, the C^2 signal provides valuable insights into the electronic structure of the complexes. This resonance progressively shifts to higher frequencies from the chlorine to the iodine derivative, with signals observed at **178.7**, **179.0**, and **180.9** ppm for **[Cu(IPr)Cl]**, **[Cu(IPr)Br]**, and **[Cu(IPr)I]**, respectively. While the chemical shift differences between the chlorine and bromine derivatives are minimal, the iodine derivative shows a significant shift ($\Delta = 2.2$ ppm). This trend reflects the increasing donor strength and atomic radius of the halides in the sequence I > Br > Cl. The shift to higher frequencies suggests an increase in the covalency and bond length of the Cu—X interaction. Although iodine is the most donating ligand, the C^2 carbon of the NHC is still more deshielded in the iodide complex, likely due to iodine's higher polarizability.[12,27]

High-resolution electrospray ionization mass spectrometry of compounds **[Cu(IPr)Cl], [Cu(IPr)Br], and [Cu(IPr)I]** are presented in Figures S13, S14, and S15, respectively. The mass spectrum of all compounds shows the *m/z* 492.2442 $[Cu(IPr)(CH_3CN)]^+$ ion as the main signal, showing the exchange of ligand X^- for CH_3CN (used as solvent). It is possible to observe a monocharged signal of 939.3990 *m/z*, of very low abundance, which shows the isotopic pattern of $[(IPr)Cu(\mu\text{-}CH_3CN)Cu(IPr)]^+$ (Figure S15), but it's only observed in the mass spectrum, which could strongly indicate an artifact of the technique.

3.2. DFT Calculations

The structural parameters of the optimized geometries show that the Cu—C bond lengths are similar across all three complexes, averaging 1.9 Å, which aligns with reported crystallographic data for **[Cu(IPr)Cl]** (1.953 Å).[44] Additionally, the optimized structure of **[Cu(IPr)Cl]** is consistent with the experimental Cu—Cl bond length (2.1 Å) and C—Cu—Cl bond angle (179.6°) (Table S1).

Bader atomic charges were calculated using the Multiwfn program, based on the electronic densities obtained from the optimized structures. The charge values (Table S2) reveal the influence of halide substitution on the charge distribution within the complexes. Notably, the positive charge on the NHC C^2 carbon, bonded to Cu(I), increases in the order **[Cu(IPr)Cl]** < **[Cu(IPr)Br]** < **[Cu(IPr)I]**, consistent with the observed ^{13}C NMR downfield shifts for these molecules, where the iodine analogue exhibits the least shielded carbon.

Additionally, the halide charges in the complexes follow the trend $Cl^- < Br^- < I^-$, indicating that iodine is the least negative,

Table 1. Percentage of DPPH reduction, calculated by Equation (2) of 100 μM (1) and 50 μM of (2)-(6) and BHT at 30 min.

Samples	A_{517nm} ± SD	Reduction (%)
DPPH	0.51 ± 0.03	–
[Cu(IPr)Cl]	0.34 ± 0.03	33.13
[Cu(IPr)Br]	0.28 ± 0.00	44.54
[Cu(IPr)I]	0.24 ± 0.02	52.03
BHT	0.27 ± 0.02	46.12

suggesting a greater ability to donate electron density to the Cu(I) center. This is further supported by the Cu(I) atomic charge, which follows the trend **[Cu(IPr)Cl]** > **[Cu(IPr)Br]** > **[Cu(IPr)I]**, with the iodine complex exhibiting the lowest positive charge. These findings align with Huynh's observations,[45] where in $[PdBr_2(iPr_2\text{-bimy})L]_n$ complexes, the ^{13}C NMR shifts of iPr_2-bimy shifted downfield as the trans ligand's electron-donating ability increased.

Based on the obtained results, the frontier orbital energies of the complexes were also analyzed (Figure S16). The energy HOMO-LUMO GAPs are 10.42, 10.44, and 10.17 eV for **[Cu(IPr)Cl]**, **[Cu(IPr)Br]**, and **[Cu(IPr)I]**. While the difference between **[Cu(IPr)Cl]** and **[Cu(IPr)Br]** is minimal, the **[Cu(IPr)I]** has a lower GAP. The LUMO orbitals of the complexes show significant orbital contribution on the copper center, suggesting that nucleophilic attack is likely directed at the metal. This electronic feature may facilitate ligand exchange reactions, in which the incoming nucleophile displaces the halide coordinated to the copper. Furthermore, in Figure S12, it is noticeable that the HOMO shape of the iodide complex differs from those of the chloride and bromide complexes. This reflects an inversion in the ordering of the occupied molecular orbitals. In the iodide complex, the HOMO has a greater contribution from the iodide ligand, whereas in the other complexes, the HOMO is more localized on the C—Cu bond.

3.3. Antioxidant Activity of Copper Complexes

DPPH (2,2-Diphenyl-1-picryl-hydrazyl-hydrate) is a stable chromogenic radical used in assays to measure the antioxidant activity of molecules, governed by a HAT (hydrogen atom transfer) and SET (electron transfer) mechanism, which can be followed by spectrophotometry at 517 nm.[46–49] DMSO was the reference, while BHT was the positive control due to its well-known antioxidant activity.[50] Table 1 presents the percentage of DPPH reduction caused by **[Cu(IPr)Cl]**, **[Cu(IPr)Br]**, and **[Cu(IPr)I]** and the reference BHT calculated according to Equation (1) described in the Materials and Methods section.

The complexes show a reduction in DPPH following the order: **[Cu(IPr)Cl]** < **[Cu(IPr)Br]** < **[Cu(IPr)I]**. Notably, the bromine derivative shows values similar to those of BHT, while **[Cu(IPr)I]** demonstrates superior activity. These findings align with previous studies, which suggest that the release of the bound halide increases with ionic radius (Cl^- < Br^- < I^-), with iodine acting as the leaving group for substitution reactions in NHC-M(I) complexes. Since the DPPH radical accepts either an electron or a hydrogen atom for reduction, we propose that copper is transferring an electron, forming Cu(II) species with ligand release, while hydrogen transfer is less likely in these complexes.[29] These results confirm the significant redox activity of the complexes.

3.4. Interaction with Bovine Serum Albumin (BSA)

Albumins are multifunctional proteins responsible for transporting a variety of endogenous and exogenous ligands through the formation of adducts. Bovine serum albumin (BSA) is commonly employed in biomimetic studies as a substitute for human serum albumin (HSA) due to its high structural homology and the lower cost of BSA. Similar to HSA, BSA exhibits intrinsic fluorescence with an emission maximum of around 345 nm, primarily attributed to its two tryptophan residues: Trp134, located on the surface of subdomain IB, and Trp212, situated within a hydrophobic binding pocket in subdomain IIA. In addition, Cys34 is a thiolate group highly reactive with metals and disulfides, near to the binding sites of BSA.[51,52] The interaction of BSA with metal complexes typically results in fluorescence quenching of the protein.[53] The mechanism of quenching can be assigned to the formation of a complex in the fundamental state, but also quenching by interaction with the excited state.

In the present study, the interactions of the compounds **[Cu(IPr)Cl]**, **[Cu(IPr)Br]**, and **[Cu(IPr)I]** with BSA were investigated by monitoring the quenching of BSA fluorescence at 350 nm. The fluorescence emission spectra and corresponding Stern–Volmer analyses are provided in Figures S17, S18, and S19, respectively. The Stern–Volmer constants (K_{SV}), calculated using Equation (2), are presented in Table 2.

The linear Stern–Volmer plots (Figures S17–S19) suggest the presence of a single quenching mechanism, either static (resulting from the formation of a non-fluorescent complex between the protein and the metal complex in the ground state) or dynamic (occurring through collisional interactions during the excited-state lifetime of the protein). The K_{SV} values obtained for the BSA–[compound] systems are on the order of 10^3 M^{-1}, indicating weak interaction between the copper complexes and BSA. The difference among the complexes is not significant, and we can say they have similar K_{SV} constant. The data agrees with previous evaluation.[20] The stoichiometric binding number (*n*) for all complexes was approximately 1, indicating that one molecule of each copper complex is bound per BSA molecule.

3.5. Lipophilicity

Lipophilicity was evaluated for complexes **[Cu(IPr)Cl]**, **[Cu(IPr)Br]**, and **[Cu(IPr)I]** using the *n*-octanol:water partition coefficient expressed as a logarithm (log *P*), using shake flask methodology.[32] An ideal lipophilic/hydrophilic balance is essential for the drug activity of the compounds. Also, log *P* is an informative parameter of the distribution tendency of a substance between apolar structures (cell membranes, for

Table 2. Stern-Volmer constant (Ksv, Equation (2)) for compounds **[Cu(IPr)Cl]**, **[Cu(IPr)Br]**, and **[Cu(IPr)I]**. Binding parameters, *n*, and Kb, for the BSA system with compounds **[Cu(IPr)Cl]**, **[Cu(IPr)Br]**, and **[Cu(IPr)I]**.

Compound	R^2	Ksv (10^3 M^{-1})	R^2	Kb (10^4 M^{-1})	n	log*P*± SD
[Cu(IPr)Cl]	0.98	6.73	0.99	0.45	1.12	−0.68 ± 0.05
[Cu(IPr)Br]	0.99	7.53	0.98	2.24	1.13	−0.36 ± 0.16
[Cu(IPr)I]	0.99	7.86	0.99	0.42	1.18	−0.22 ± 0.03

Table 3. EC_{50} calculated for the compounds against promastigotes of *L. amazonensis* (± standard deviation). CC_{50} determined for BMDM. The Selectivity index (SI) calculated as CC_{50}/EC_{50}.

Compound	[Cu(IPr)Cl]	[Cu(IPr)Br]	[Cu(IPr)I]
EC_{50} (μM)	2.4 ± 0.4	1.9 ± 0.1	1.5 ± 0.4
CC_{50} (μM)	2.8 ± 0.4	4.3 ± 0.4	6.0 ± 0.8
SI	1.2	2.3	4.0

Table 4. Effects of the compounds on Vero-E6 viability (CC_{50}) and CHIKV replication (EC_{50}). The selectivity index (SI) was calculated by the ratio CC_{50}/EC_{50}.

Compound	[Cu(IPr)Cl]	[Cu(IPr)Br]	[Cu(IPr)I]
EC_{50} (μM)	0.782	0.807	1.807
CC_{50} (μM)	1.983	3.892	3.297
SI	2.54	4.83	1.83

example) and aqueous solutions (blood plasma and others).[54,55] Table 2 presents the experimental log *P* values for the compounds **[Cu(IPr)Cl]**, **[Cu(IPr)Br]**, and **[Cu(IPr)I]**. The partitioning was quantified by measuring copper in the aqueous phase using ICP-OES, with the corresponding calibration curve provided in Figure S20.

The **[Cu(IPr)X]** compounds exhibited negative log P values close to zero, indicating a slight hydrophilicity. The hydrophilicity-lipophilicity trend follows the halogen series, with chloride being the most hydrophilic (—0.684) and iodine the most lipophilic (—0.216).

3.6. Leishmanicidal Activity

The antileishmanial activity against *Leishmania amazonensis* promastigotes (5×10^6 parasites/well) and the cytotoxicity toward host cells were evaluated using bone marrow-derived macrophages (BMDMs, 5×10^4 cells/well). Both parasite viability and host cell viability were assessed following 24 h of incubation with serial dilutions of the tested compounds at concentrations ranging from 25 to 0.625 μM. The half-maximal effective concentration (EC_{50}) and half-maximal cytotoxic concentration (CC_{50}) values were determined from concentration–response curves. The results are summarized in Table 3.

Although the compounds exhibited activity against promastigotes, they demonstrated toxicity toward BMDMs, resulting in low selectivity indices (SI). In the context of novel metallodrug development, comparative analysis revealed significant differences in the SI values among the tested complexes.[10,20] The incorporation of iodine proved advantageous in the design of these complexes. Factors potentially contributing to these findings include the electronic properties of the Cu—I bond and the increased lipophilicity of the iodinated complexes, which were evaluated and discussed in this work.

The incorporation of iodine proved beneficial in the design of these complexes. Potential factors contributing to these findings include the electronic properties of the Cu—I bond, the increased lipophilicity of the iodinated complexes, and the role of the ligand scaffolds. These factors, in combination, appear to be significant in improving drug efficacy and selectivity.

3.7. Antiviral Activity Assay

The antiviral activity against chikungunya virus and the cytotoxicity toward host cells were evaluated using Vero-E6 cell line. Both viral inhibition and host cell viability were assessed following 24 h of incubation with serial dilutions of the tested compounds. Curves are presented in Figure S21.The effective concentration of 50% (EC_{50}) and cytotoxic concentration of 50% (CC_{50}) values were determined from concentration–response curves (Figure S21). The values of CC_{50} and EC_{50} were used to calculate the selectivity index ($SI = CC_{50}/EC_{50}$). The results are summarized in Table 4.

The compounds effectively inhibit CHIKV replication. In this study, we used the data to compare these compounds and address the challenges in novel drug development.

Among the halogen series, **[Cu(IPr)Cl]** was the most toxic, while **[Cu(IPr)Br]** and **[Cu(IPr)I]** had similar cytotoxic concentration profiles (CC_{50}), with **[Cu(IPr)Br]** being slightly less toxic than its iodine counterpart. In terms of viral replication inhibition, the effectiveness followed the order: **[Cu(IPr)Cl]** ≈ **[Cu(IPr)Br]** > **[Cu(IPr)I]**, with the chloride and bromide showing nearly identical EC_{50} values. Interestingly, the presence of iodine did not enhance the antiviral effect; instead, it worsened replication inhibition.

Therefore, among the tested compounds, bromine proved to be the most promising for anti-CHIKV development, with **[Cu(IPr)Br]** standing out in SI analysis, with a significant value.

4. Conclusions

In this study, we investigated the activity and properties of three metal-based compounds—**[Cu(IPr)Cl]**, **[Cu(IPr)Br]**, and

[Cu(IPr)I]—to assess the influence of halogen substitution on anti-*Leishmania* and antiviral activity. Our findings reveal that halogen variation significantly impacts both chemical behavior and biological performance. Carbon NMR analysis, supported by DFT studies, indicated that iodine forms a more covalent bond due to its high polarizability, leading to greater NHC C^2 deshielding and lower HOMO–LUMO gap, demonstrating it is more susceptible to nucleophilic attack. This effect was less pronounced in the chloride and bromide derivatives, which exhibited similar electronic environments. Additionally, **[Cu(IPr)I]** demonstrated the highest antioxidant activity in DPPH assays and the greatest lipophilicity. Biologically, the iodine derivative displayed the highest anti-*Leishmania* potency, coupled with lower toxicity to host cells, resulting in an improved selectivity index (SI). This suggests that lipophilicity and the nature of the Cu—I bond may play key roles in its enhanced activity. In contrast, antiviral activity did not follow the same profile. While **[Cu(IPr)I]** exhibited lower host cell toxicity compared to **[Cu(IPr)Cl]** and similar toxicity to **[Cu(IPr)Br],** its potency in inhibiting CHIKV replication was the weakest. This indicates that factors beyond lipophilicity, antioxidant activity, and Cu–X bond characteristics influence antiviral efficacy. Among the tested compounds, **[Cu(IPr)Br]** demonstrated the highest SI against CHIKV, improving upon the previously observed effects of **[Cu(IPr)Cl]** by reducing host cell toxicity.

Overall, this study highlights the critical role of halogen substitution in modulating the bioactivity of organometallic compounds and underscores the potential of fine-tuning these properties for drug development.

Acknowledgments

This study was supported by Fundação de Amparo à Pesquisa do Estado de São Paulo (FAPESP) Grants # 2022/02618–0, 2022/06410-5, 2023/12657–6 and Conselho Nacional de Desenvolvimento Científico e Tecnologicó (CNPq) Grant # 404668/2021–6 and PQ 304587/2022–2. DCM thanks CNPq PQ 314811/2021–4. We thank Centro Nacional de Processamento de Alto Desempenho em São Paulo (CENAPAD) Project #638 for computational resources and support. MEFA thanks CNPq and Unicamp Research Deen for the scholarship. MSAG thanks Coordenação de Aperfeiçoamento de Pessoal de Nível Superior (CAPES) # 88887.713008/2022–00 for the scholarship. ACGJ is grateful to Fundação de Amparo à Pesquisa do Estado de Minas Gerais (FAPEMIG) APQ-01487–22 and APQ-04686–22, CNPq Grant # 409187/2023–2, and to CAPES (Prevention and Combat of Outbreaks, Endemics, Epidemics and Pandemics—Finance Code #88881.506794/2020–01 and—Finance Code 001). We thank Andres Merits (Institute of Technology, University of Tartu, Tartu, Estonia) for the provision of the CHIKV expressing-nanoluciferase.

The Article Processing Charge for the publication of this research was funded by the Coordenacao de Aperfeicoamento de Pessoal de Nivel Superior - Brasil (CAPES) (ROR identifier: 00x0ma614).

Conflict of Interests

The authors declare no conflicts of interest.

Author Contributions

J.V.F.: Conceptualization; formal analysis; writing and supervision; **M.E.F.A.**: Investigation; formal analysis (chemical and biophysical data) and writing. **G.C.R.**: Investigation; formal analysis (DFT calculations) and writing. **M.S.A.G.** and **A.V.P.F.**: Investigation; formal analysis (anti-*Leishmania* investigation) and writing; **G.A.A.** and **A.L.C.O.**: Investigation; formal analysis (antiviral investigation) and writing; **D.C.M.**: Supervision; data curation and writing (review and editing);funding acquisition and supervision; **A.C.G.J.**: Supervision; data curation and writing (review and editing); funding acquisition and supervision; **C.A.**: Conceptualization; data curation; writing—review and editing; funding acquisition and supervision.

Data Availability Statement

The data that support the findings of this study are available on request from the corresponding author. The data are not publicly available due to privacy or ethical restrictions.

Keywords: Copper compounds · Halogen · Neglected diseases · *N*-heterocyclic carbenes

[1] C. Abbehausen, M. S. A. Garcia, J. V. Fontes, B. E. S. da Silva, F. R. Gadelha, D. C. Miguel, *Integr. Sci.* **2024**, *25*, 187–208.
[2] M. S. A. Garcia, V. A. Oliveira Filho, M. B. C. Brioschi, K. Minori, D. C. Miguel, *Trends Parasitol* **2025**, *41*, 66–67.
[3] L. M. Alcântara, T. C. S. Ferreira, F. R. Gadelha, D. C. Miguel, *Int. J. Parasitol Drugs Drug Resist.* **2018**, *8*, 430–439.
[4] Center for Disease Control, and Prevention (CDC), Chikungunya virus, https://www.cdc.gov/chikungunya/index.html.
[5] Fiocruz, Chikungunya: sintomas transmissão e prevenção, https://www.bio.fiocruz.br/index.php/br/chikungunya-sintomas-transmissao-e-prevencao.
[6] P. G. Jupp, B. M. McIntosh, in *The Arboviruses*, 1st ed., CRC Press, Boca Raton, **1988**, p. 21.
[7] L. A. Silva, T. S. Dermody, *J. Clin. Invest.* **2017**, *127*, 737–749.
[8] R. L. Aires, I. A. Santos, J. V. Fontes, F. R. G. Bergamini, A. C. G. Jardim, C. Abbehausen, *Metallomics* **2022**, *14*, mfac056.
[9] L. S. Oliveira, L. B. Rosa, D. D. Affonso, I. A. Santos, J. C. da Silva, G. C. Rodrigues, M. Harris, A. C. G. Jardim, D. H. Nakahata, J. R. Sabino, J. E. de Carvalho, D. C. Miguel, A. L. T. G. Ruiz, C. Abbehausen, *ChemBioChem* **2023**, *25*, e202300696.
[10] L. B. Rosa, C. Galuppo, R. L. A. Lima, J. V. Fontes, F. S. Siqueira, W. A. S. Júdice, C. Abbehausen, D. C. Miguel, *J. Inorg. Biochem.* **2022**, *229*, 111726.
[11] L. B. Rosa, R. L. Aires, L. S. Oliveira, J. V. Fontes, D. C. Miguel, C. Abbehausen, *ChemMedChem* **2021**, *16*, 1682–1696.
[12] I. S. Oliveira, M. S. A. Garcia, N. M. Cassani, A. L. C. Oliveira, L. C. F. Freitas, V. K. S. Bertolini, J. Castro, G. Clauss, J. Honorato, F. R. Gadelha, D. C. Miguel, A. C. G. Jardim, C. Abbehausen, *Dalton Trans.* **2024**, *53*, 18963–18973.
[13] A. Binesh, K. Venkatachalam, *J. Biochem. Mol. Toxicol.* **2024**, *38*, e70052.
[14] S. K. Mustafa, M. A. AlSharif, *Am. J. Analyt. Chem.* **2018**, *09*, 15–26.
[15] A. A. Danopoulos, T. Simler, P. Braunstein, *Chem. Rev.* **2019**, *119*, 3730–3961.

[16] M. L. Teyssot, A. S. Jarrousse, A. Chevry, A. De Haze, C. Beaudoin, M. Manin, S. P. Nolanilvia, Díez-González, L. Morel, A. Gautier, *Chem. – A European J.* **2009**, *15*, 314–318.
[17] M. Elie, F. Sguerra, F. Di Meo, M. D. Weber, R. Marion, A. Grimault, J. F. Lohier, A. Stallivieri, A. Brosseau, R. B. Pansu, J. L. Renaud, M. Linares, M. Hamel, R. D. Costa, S. Gaillard, *ACS Appl. Mater. Interfaces* **2016**, *8*, 14678–14691.
[18] N. Touj, I. S. A. Nasr, W. S. Koko, T. A. Khan, I. Özdemir, S. Yasar, L. Mansour, F. Alresheedi, N. Hamdi, *J. Coord. Chem.* **2020**, *73*, 2889–2905.
[19] N. Touj, A. Chakchouk-Mtibaa, L. Mansour, A. H. Harrath, J. Al-Tamimi, L. Mellouli, I. Özdemir, S. Yasar, N. Hamdi, *J. Mol. Struct.* **2019**, *1181*, 209–219.
[20] J. V. Fontes, I. A. Santos, L. B. Rosa, R. L. A. Lima, A. C. G. Jardim, D. C. Miguel, C. Abbehausen, *ChemistrySelect* **2022**, *7*, e202201560.
[21] L. dos Santos Oliveira, P. H. de Souza Guarda, L. B. Rosa, G. C. Rodrigues, D. D. Affonso, J. E. de Carvalho, I. A. Santos, M. Harris, D. H. Nakahata, J. R. Sabino, D. C. Miguel, A. L. T. G. Ruiz, A. C. G. Jardim, C. Abbehausen, *Inorganica. Chim. Acta* **2024**, *560*, 121806.
[22] I. Landini, L. Massai, D. Cirri, T. Gamberi, P. Paoli, L. Messori, E. Mini, S. Nobili, *J. Inorg. Biochem.* **2020**, *208*, 111079.
[23] T. Marzo, L. Massai, A. Pratesi, M. Stefanini, D. Cirri, F. Magherini, M. Becatti, I. Landini, S. Nobili, E. Mini, O. Crociani, A. Arcangeli, S. Pillozzi, T. Gamberi, L. Messori, *ACS Med. Chem. Lett.* **2019**, *10*, 656–660.
[24] C. M. Teles, L. C. Lammoglia, M. A. Juliano, A. L. T. G. Ruiz, T. Z. Candido, J. E. de Carvalho, C. S. P. Lima, C. Abbehausen, *J. Inorg. Biochem.* **2019**, *199*, 110754.
[25] D. Cirri, I. Landini, L. Massai, E. Mini, F. Maestrelli, L. Messori, *Pharmaceutics* **2021**, *13*, *727*.
[26] A. Annunziata, G. Ferraro, M. E. Cucciolito, P. Imbimbo, A. Tuzi, D. M. Monti, A. Merlino, F. Ruffo, *Dalton Trans.* **2022**, *51*, 10475–10485.
[27] S. K. Goetzfried, P. Kapitza, C. M. Gallati, A. Nindl, M. Cziferszky, M. Hermann, K. Wurst, B. Kircher, R. Gust, *Dalton Trans.* **2022**, *51*, 1395–1406.
[28] B. Bertrand, L. Stefan, M. Pirrotta, D. Monchaud, E. Bodio, P. Richard, P. Le Gendre, E. Warmerdam, M. H. De Jager, G. M. M. Groothuis, M. Picquet, A. Casini, *Inorg. Chem.* **2014**, *53*, 2296–2303.
[29] M. Hans, J. Lorkowski, A. Demonceau, L. Delaude, *Beilstein J. Org. Chem.* **2015**, *11*, 2318–2325.
[30] O. Santoro, A. Collado, A. M. Z. Slawin, S. P. Nolan, C. S. J. Cazin, *Chem. Commun.* **2013**, *49*, 10483.
[31] OECD/OCDE, Guidance. **1995**, *107*, 1–4.
[32] M. H. M. Klose, S. Theiner, H. P. Varbanov, D. Hoefer, V. Pichler, M. Galanski, S. M. Meier-Menches, B. K. Keppler, *Inorganics (Basel)* **2018**, *6*, 130.
[33] V. A. de Oliveira Filho, M. S. A. Garcia, L. B. Rosa, S. Giorgio, D. C. Miguel, *Parasitologia* **2024**, *4*, 305–318.
[34] P. Kumar, A. Nagarajan, P. D. Uchil, *Cold Spring Harb. Protoc.* **2018**, *2018*, 469–471.
[35] R. Matkovic, E. Bernard, S. Fontanel, P. Eldin, N. Chazal, D. Hassan Hersi, A. Merits, J.-M. Péloponèse, L. Briant, *J. Virol.* **2019**, *93*, e01764-18.
[36] F. Neese, F. Wennmohs, U. Becker, C. Riplinger, *J. Chem. Phys.* **2020**, *152*, 224108.
[37] N. Mardirossian, M. Head-Gordon, *Phys. Chem. Chem. Phys.* **2014**, *16*, 9904.
[38] J. D. Rolfes, F. Neese, D. A. Pantazis, *J. Comput. Chem.* **2020**, *41*, 1842–1849.
[39] S. Kossmann, F. Neese, *J. Chem. Theo. Comput.* **2010**, *6*, 2325–2338.
[40] M. Garcia-Ratés, F. Neese, *J. Comput. Chem.* **2019**, *40*, 1816–1828.
[41] M. Garcia-Ratés, F. Neese, *J. Comput. Chem.* **2020**, *41*, 922–939.
[42] T. Lu, *J. Chem. Phys.* **2024**, *161*, 082503.
[43] A. J. Arduengo, Preparation of 1,3-Disubstituted Imidazolium Salts, US Pat 5,077,414, **1991**.
[44] H. V. Huynh, Y. Han, R. Jothibasu, J. A. Yang, *Organometallics* **2009**, *28*, 5395–5404.
[45] H. Kaur, F. K. Zinn, E. D. Stevens, S. P. Nolan, *Organometallics* **2004**, *23*, 1157–1160.
[46] I. G. Munteanu, C. Apetrei, *Int. J. Mol. Sci.* **2021**, *22*, 3380.
[47] V. Jirjees, V. Suleman, S. Ahmed, A. Al-Hamdani, *The J. Univer. Duhok* **2020**, *23*, 41–50.
[48] A. Fadda, M. Serra, M. G. Molinu, E. Azara, A. Barberis, D. Sanna, *J. Food Compos. Anal.* **2014**, *35*, 112–119.
[49] İ. Gulcin, S. H. Alwasel, *Processes* **2023**, *11*, 2248.
[50] V. Mishra, R. J. Heath, *Int. J. Mol. Sci.* **2021**, *22*, 8411.
[51] S. Sengupta, H. Chen, T. Togawa, P. M. DiBello, A. K. Majors, B. Büdy, M. E. Ketterer, D. W. Jacobsen, *J. Biol. Chem.* **2001**, *276*, 30111–30117.
[52] W. Bal, M. Sokołowska, E. Kurowska, P. Faller, *Biochim. Biophys. Acta Gen. Subj.* **2013**, *1830*, 5444–5455.
[53] A. Berthod, S. Carda-Broch, *J. Chromatogr. A* **2004**, *1037*, 3–14.
[54] C. Giaginis, F. Tsopelas, A. Tsantili-Kakoulidou, in *Rational Drug Design*, (Eds.: T. Mavromoustakos, T. Kellici), Methods in Molecular Biology, **2018**, *1824*, pp. 217–228.

Manuscript received: April 4, 2025